Autonomous Ground Vehicle Control System for High-Speed and Safe Operation

Junmin Wang*, *Member, IEEE,*   Joe Steiber,   Bapiraju Surampudi, *Senior Member, IEEE*

Abstract— **This paper describes a new trajectory tracking control system for autonomous ground vehicles (AGV) toward safe and high-speed operation enabled by incorporating vehicle dynamics control (VDC) into the AGV. The control system consists of two levels: an AGV desired yaw rate generator based on a kinematic model, and a yaw rate controller based on the vehicle/tire dynamic models. The separation between AGV trajectory tracking and low-level actuation allows the incorporation of the VDC into the AGV systems. Sliding mode control is utilized to handle the system uncertainties. The performance of the proposed control system is evaluated by using a high-fidelity (experimentally validated) full-vehicle sport utility vehicle (SUV) model (rear-drive and front-steer) provided by CarSim® on a race track. Compared with the results for typically-employed position error based AGV control, significant performance improvement is observed.**

Index Terms – **Autonomous ground vehicle, high-speed operation, trajectory tracking, vehicle dynamics control.**

I. INTRODUCTION

AUTONOMOUS ground vehicle technology has become a rapidly growing research area attracting significant effort from both academia and industry [1-6]. For AGV systems, it is required that the vehicle can automatically manipulate its actuation to precisely follow a predefined or dynamically routed trajectory for single-vehicle tasks or multi-vehicle cooperation. Several different AGV trajectory tracking control approaches have been proposed in the literature. In [2], Tan et al. reported an autonomous vehicle trajectory tracking approach by combining way point guidance and model reference control law for the under-actuated autonomous vehicles. Hoffmann et al. [3] designed a nonlinear control law for AGV trajectory tracking by controlling the orientation of the front wheels and demonstrated on a passenger vehicle for off-road operation. A preview steering control law is proposed and experimentally demonstrated by Rajamani et al. [4] for low speed automated operation on a backward driven front-steering truck. In [5], authors used sliding mode control to manipulate the AGV steering for position tracking. However, in some of the above AGV trajectory tracking control literature, vehicle dynamics were not specifically addressed. For high-speed operation and severe maneuvers, vehicle dynamics plays a vital role for driving safety and vehicle stability. In order to expand the AGV

operational envelope (the main criterion being AGV traveling speed, which is often limited by severe maneuvers such as sharp turns and adverse driving conditions), vehicle dynamics needs to be taken into account.

In this paper, instead of directly connecting the vehicle steering to the position tracking error as most of the AGV controllers do, we propose a new AGV control system in which vehicle yaw rate, the most important state for VDC, is actively controlled to achieve trajectory tracking while maintaining vehicle stability at severe maneuvers and under adverse conditions. The separation between position tracking and steering also makes it possible to incorporate some advanced vehicle dynamics control systems such as differential braking, torque vectoring as well as coordinated vehicle dynamics control [7-11] into the AGV system, and therefore, expand its operational envelope. The system architecture is shown in Fig. 1. Based on the desired AGV position, actual position and vehicle planar motions, the desired yaw rate is generated. The desired yaw rate is sent (as a reference signal) to the yaw rate tracking controller, where steering and potentially differential braking and/or torque vectoring systems are manipulated to make the actual yaw rate track the desired one. Additional AGV sensing systems such as camera, lidar, GPS/IMU etc. can be used to provide critical/necessary information on vehicle and environment. The sensor information is passed to the yaw rate tracking controller, upper-level decision maker and path planner. In the trajectory tracking algorithm presented in this paper, only the signals from GPS/IMU are used.
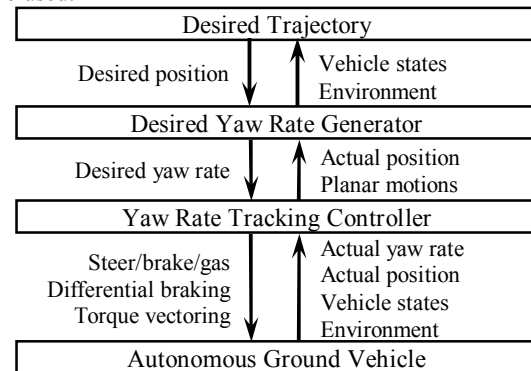

Fig. 1. System architecture for high-speed AGV.

This paper is organized as follows. The desired yaw rate generation is developed in section II. AGV yaw rate tracking controller is described in section III and evaluation of simulation results are presented in section

IV. Finally, future work and conclusive remarks are given in section V.

II. DESIRED YAW RATE GENERATION

In this section, the AGV desired yaw rate is generated based on a kinematic model for trajectory tracking.

A. Kinematic Model for AGV Trajectory Tracking

In an inertial frame, vehicle's global position and heading $(X \ \ Y \ \ \psi)^T$ are determined by the following kinematic equations of motion as,

$$\dot{X} = V_x \cos(\psi) - V_y \sin(\psi), \tag{1a}$$

$$\dot{Y} = V_x \sin(\psi) + V_y \cos(\psi), \tag{1b}$$

$$\dot{\psi} = r, \tag{1c}$$

where V_x and V_y are the body-fixed vehicle longitudinal and lateral velocities, respectively. The yaw rate at vehicle center of gravity (CG) is denoted by r. The system is nonholonomic.

The AGV global position and heading errors can be defined as,

$$X_e = X_d - X, \tag{2a}$$

$$Y_e = Y_d - Y, \tag{2b}$$

$$\psi_e = \psi_d - \psi, \tag{2c}$$

where X_d, Y_d, and ψ_d are the desired AGV position and heading from the path planner. These tracking errors denoted in the inertial frame can be transformed to the AGV frame as [12]

$$\begin{pmatrix} x_e \\ y_e \\ \psi_e \end{pmatrix} = \begin{bmatrix} \cos(\psi) & \sin(\psi) & 0 \\ -\sin(\psi) & \cos(\psi) & 0 \\ 0 & 0 & 1 \end{bmatrix} \begin{pmatrix} X_e \\ Y_e \\ \psi_e \end{pmatrix}. \tag{3}$$

In this paper, we consider the trajectory tracking as the AGV lateral position and yaw/heading tracking control. A separate controller is used to track the vehicle longitudinal speed.

B. Yaw Rate Generation for Trajectory Tracking

As the AGV local lateral position (to the reference trajectory) is the main tracking control objective, we can design a control law to specify the AGV desired yaw rate for minimizing the lateral position error. If we take the time derivative of y_e and set it as $\dot{y}_e = -\lambda_1 y_e$, where $\lambda_1 \in \Re^+$ is the control gain, we can get the following equation,

$$-\sin(\psi)\dot{X}_d + \cos(\psi)\dot{Y}_d - V_y$$
$$= \lambda_1 \sin(\psi) X_e - \lambda_1 \cos(\psi) Y_e \tag{4}$$

Typically, vehicle lateral velocity is much smaller than its longitudinal velocity. If we ignore the lateral velocity, then a vehicle heading that can ensure the asymptotical stability of the lateral position error is

$$\psi_{r0} = \text{atan}\left(\frac{\dot{Y}_d + \lambda_1 Y_e}{\dot{X}_d + \lambda_1 X_e}\right). \tag{5}$$

Here, the ψ_{r0} serves as a virtual control at this level. Notice that the heading value calculated from (5) will have a jump of π when ψ_{r0} crosses $\pm\left(l+\frac{1}{2}\right)\pi$, $l = 0,1,2,...$ (occurs when $\dot{X}_d + \lambda_1 X_e \to 0$). Practically, based on the continuity of the vehicle heading, the following filter can remove the associated discontinuities,

$$\psi_{r0}(i) = \begin{cases} \psi_{r0}(i), & |\psi_{r0}(i) - \psi_{r0}(i-1)| \le \theta_t \\ \psi_{r0}(i) + sign(\psi_{r0}(i-1))\pi, & |\psi_{r0}(i) - \psi_{r0}(i-1)| > \theta_t \end{cases}, \tag{6}$$

with θ_t being the threshold value such as $\pi/2$.

As (5) is derived by ignoring the vehicle lateral velocity, some tracking error may be introduced especially during turning maneuvers. To reduce this disturbance effect, a small feedback term could be added to (5) as

$$\psi_r = \psi_{r0} + ky_e. \tag{7}$$

Once the desired vehicle heading or yaw angle is specified, the commanded vehicle yaw rate can be generated. The AGV heading/yaw dynamics is governed by (1c). Different methods can be used to produce the commanded yaw rate for achieving the desired vehicle heading. For example, the following simple control law can satisfy the task.

$$r_r = \dot{\psi}_r + \lambda_2(\psi_r - \psi), \quad \lambda_2 \in \Re^+ \tag{8}$$

where r_r is the reference yaw rate for the lower-level vehicle controller, and λ_2 is the control gain.

III. AGV YAW RATE CONTROLLER DESIGN

Since only the regular driving/braking/steering systems are available on the current AGV platform, in this paper, the yaw rate control is realized by manipulating the steering hand-wheel. However, advanced vehicle dynamics control systems such as differential braking and torque vectoring can be readily incorporated into the control architecture.

A. Vehicle Dynamic Modeling

Vehicle planar motions (longitudinal speed, lateral speed, and yaw rate) as shown in Fig. 2 are of the most interest for vehicle dynamic control.
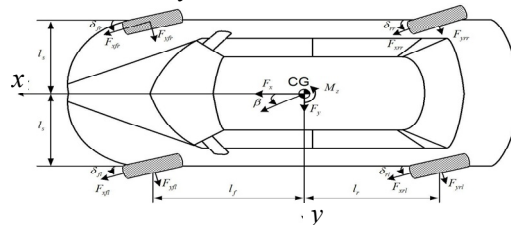

Fig. 2 The ground vehicle planar dynamic motion.

The simplified equations of motion for the vehicle dynamics can be written as,

$$m_v(\dot{V}_x - rV_y) = F_x \tag{9a}$$

$$m_v(\dot{V}_y + rV_x) = F_y, \tag{9b}$$

$$I_z \dot{r} = M_z \tag{9c}$$

where m_v is the vehicle mass (including both sprung and

unsprung mass), V_x is vehicle velocity along the x axis, V_y is vehicle velocity along the y axis, and I_z is moment of inertia about the z axis, which is perpendicular to the xy plane. The coordinates x, y, z are body-fixed at the center of gravity of the vehicle. The generalized external forces acting along the vehicle X and Y axes are F_x and F_y, and the generalized moment is M_z about the Z axis. Ultimately, each of the four tires can independently drive, brake, and steer (*The AGV platform in this paper only has front-steer and rear-drive*). Thus these generalized forces/moment are expressed as,

$$F_x = F_{xfl}\cos\delta_{fl} - F_{yfl}\sin\delta_{fl} + F_{xfr}\cos\delta_{fr} - F_{yfr}\sin\delta_{fr} \\ + F_{xrl}\cos\delta_{rl} - F_{yrl}\sin\delta_{rl} + F_{xrr}\cos\delta_{rr} - F_{yrr}\sin\delta_{rr} \tag{10a}$$

$$F_y = F_{xfl}\sin\delta_{fl} + F_{yfl}\cos\delta_{fl} + F_{xfr}\sin\delta_{fr} + F_{yfr}\cos\delta_{fr} \\ + F_{xrl}\sin\delta_{rl} + F_{yrl}\cos\delta_{rl} + F_{xrr}\sin\delta_{rr} + F_{yrr}\cos\delta_{rr} \tag{10b}$$

$$M_z = l_s(-F_{xfl}\cos\delta_{fl} + F_{yfl}\sin\delta_{fl} - F_{xrl}\cos\delta_{rl} + F_{yrl}\sin\delta_{rl}) \\ + l_s(F_{xfr}\cos\delta_{fr} - F_{yfr}\sin\delta_{fr} + F_{xrr}\cos\delta_{rr} - F_{yrr}\sin\delta_{rr}) \\ + l_f(F_{xfl}\sin\delta_{fl} + F_{yfl}\cos\delta_{fl} + F_{xfr}\sin\delta_{fr} + F_{yfr}\cos\delta_{fr}) \\ + l_r(-F_{xrl}\sin\delta_{rl} - F_{yrl}\cos\delta_{rl} - F_{xrr}\sin\delta_{rr} - F_{yrr}\cos\delta_{rr}) \tag{10c}$$

In these relations, δ_{**} is the steering angle of a given wheel, with the first subscript representing front/rear and the second subscript right/left.

B. Tire Model

As the only vehicle components generating external forces that can be effectively manipulated to affect vehicle motions, tires are crucial for vehicle dynamics and control. Tire longitudinal force, lateral force, and aligning moment are complex nonlinear functions of tire normal force, slip, slip angle, and tire-road friction coefficient. Fig. 3 and Fig. 4 graph normalized longitudinal and lateral tire forces, respectively, as functions of slip and slip angle for tire-road friction coefficient of 0.9.

The tire model needs to describe the dependence of the tire force on the slip/slip angle, friction coefficient, tire normal force, as well as the coupling between tire longitudinal and lateral forces. The longitudinal tire slip is defined as,

$$s_i = \frac{\omega_{wyi}R_i - V_{xi}}{V_{xi}} = \frac{\omega_{wyi}R_i}{V_{xi}} - 1, \tag{11}$$

where ω_{wyi} is wheel rotational speed along wheel Y axis, V_{xi} is the longitudinal speed of the wheel center as a function of vehicle CG velocities, yaw rate and wheel steering angles, and R_i is the tire effective radius, with specified tire indicated by subscript $i \in \begin{pmatrix} fl & fr & rl & rr \end{pmatrix}$. The slip angle for each tire can be calculated as

$$\alpha_{fl} = -\delta_{fl} + \tan^{-1}\left(\frac{V_y + rl_f}{V_x - rl_s}\right), \tag{12a}$$

$$\alpha_{fr} = -\delta_{fr} + \tan^{-1}\left(\frac{V_y + rl_f}{V_x + rl_s}\right), \tag{12b}$$

$$\alpha_{rl} = -\delta_{rl} + \tan^{-1}\left(\frac{V_y - rl_r}{V_x - rl_s}\right), \tag{12c}$$

$$\alpha_{rr} = -\delta_{rr} + \tan^{-1}\left(\frac{V_y - rl_r}{V_x + rl_s}\right). \tag{12d}$$

For notational simplicity, slip angle can be represented as,

$$\alpha_i = f_{\alpha i}(\delta_i, \xi), \tag{13}$$

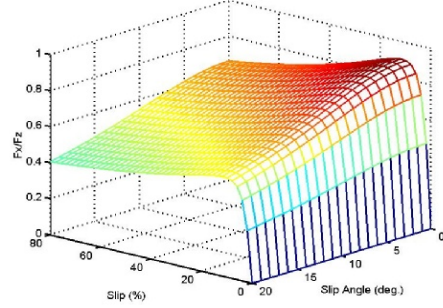with $\xi = [V_x, V_y, r]^T$ being the vehicle motion vector.

Fig. 3. Normalized tire longitudinal force as a function of slip and slip angle
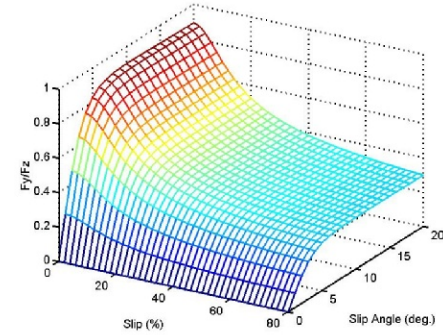

Fig. 4. Normalized tire lateral force as a function of slip and slip angle

Many tire models exist in the literature. For control simplicity, the following models can be adopted.

$$F_{xi} = F_{zi}K_x(\mu)s_i \tag{14a}$$

$$F_{yi} = F_{zi}K_y(\mu)\alpha_i \tag{14b}$$

Notice that the above simple tire model is valid when tire is not experiencing significant longitudinal and lateral forces simultaneously.

C. Tire Normal Loads

From the tire model described previously, it is clear that the amplitudes of the tire longitudinal and lateral forces directly depend on its normal force F_{zi}. The static tire normal load can be calculated from the equations,

$$F_{zfl0} = \frac{m_v g l_r}{2(l_f + l_r)}, \tag{15a}$$

$$F_{zfr0} = \frac{m_v g l_r}{2(l_f + l_r)}, \tag{15b}$$

$$F_{zrl0} = \frac{m_v g l_f}{2(l_f + l_r)}, \tag{15c}$$

$$F_{zrr0} = \frac{m_v g l_f}{2(l_f + l_r)}. \tag{15d}$$

For vehicle dynamics control systems, the effect of the load transfers due to vehicle sprung mass longitudinal and lateral accelerations will need to be considered in order to closely approximate the actual tire normal load during driving. For simplicity, assume the front and rear roll center heights of the vehicle (sprung mass and unsprung mass) are same. The dynamic load transfer of each tire can be calculated from

$$\delta F_{zfl} = -\frac{m_{vs}a_x h_g}{2(l_f + l_r)} - \frac{m_{vs}a_y h_r \kappa_f}{2l_s}, \quad (16a)$$

$$\delta F_{zfr} = -\frac{m_{vs}a_x h_g}{2(l_f + l_r)} + \frac{m_{vs}a_y h_r \kappa_f}{2l_s}, \quad (16b)$$

$$\delta F_{zrl} = \frac{m_{vs}a_x h_g}{2(l_f + l_r)} - \frac{m_{vs}a_y h_r \kappa_r}{2l_s}, \quad (16c)$$

$$\delta F_{zrr} = \frac{m_{vs}a_x h_g}{2(l_f + l_r)} + \frac{m_{vs}a_y h_r \kappa_r}{2l_s}, \quad (16d)$$

where, κ_f, κ_r are the roll stiffness factor of the front and rear suspension, respectively, and $\kappa_f + \kappa_r = 1$. In this estimation approach, the vehicle body longitudinal and lateral accelerations are needed, and these quantities can be easily measured by widely available GPS/IMU. The bias issues associated with the inertial sensors can be overcome by sensor fusion methods described in [13, 14].

D. SSTI AGV Platform

The AGV platform used for the Southwest Safe Transportation Initiative (SSTI) is a Ford/Explorer XLS as shown in Fig. 5.

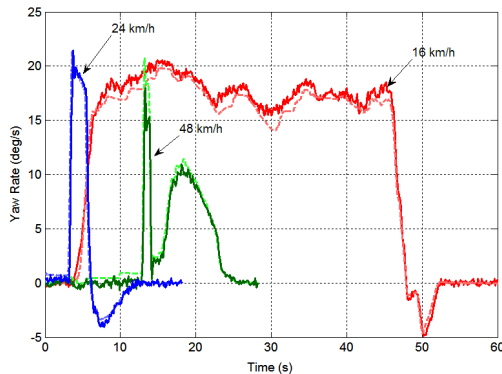

Fig. 5. The SSTI AGV vehicle and control/sensing systems.

Fig. 6. Comparisons of modeled and measured vehicle dynamics (thick solid lines: measured; thin dash lines: modeled)

Top row of Fig. 5 shows the EMC™ electronic driving system to actuate the gas/braking pedal and steering

wheel, dSPACE™ AutoBox controller, camera, GPS/IMU, and main power and computing resource installed on-board. The middle row shows the SSTI AGV vehicle. Two ibeo scanners are installed on the front bumper of the vehicle.

The AGV platform was modeled in CarSim® with the actual configuration parameters. Fig. 6 shows the comparisons of the vehicle yaw rate responses that were predicted by the CarSim® AGV model and measured on the real AGV platform using GPS/IMU during step-steering maneuvers at different vehicle speeds. As one can see, the AGV CarSim® model captures the vehicle dynamics well and therefore provides high-fidelity model for control system design purposes. Also it can be found from the comparisons that the yaw rate measurements do not noticeably subject to noise caused by sensors, vibration, and other vehicle motions.

E. Yaw Rate Sliding Mode Controller Design

For vehicles where 4-wheel driving/steering are not available, then we have $\delta_{fl} = \delta_{fr} = \delta_s$, $\delta_{rl} = \delta_{rr} = 0$. For this project, a Ford/Explorer XLS is selected as the target AGV platform. Since the vehicle has a rear wheel drive, we can ignore the longitudinal forces of the front tires and assume the longitudinal forces of the rear tires are same. With those simplifications, the yaw moment acting on vehicle CG becomes

$$M_z = l_s \sin\delta_s \left(F_{yfl} - F_{yfr}\right) + l_f \cos\delta_s \left(F_{yfl} + F_{yfr}\right) - l_r \left(F_{yrl} + F_{yrr}\right). (17)$$

For normal steering angle ranges, δ_s is small and we can have $\cos\delta_s \approx 1$ and ignore the first term in (17). We can further simplify (17) as

$$M_z = -l_r \left(F_{yrl} + F_{yrr}\right) + \Delta M + l_f \left[F_{zfl}K_y(\mu_{fl})\alpha_{fl} + F_{zfr}K_y(\mu_{fr})\alpha_{fr}\right], \quad (18)$$

where ΔM is the yaw moment caused by the ignored terms. By substituting (12) and (14) into (18), one can get

$$M_z = -l_r \left(F_{zrl}K_y(\mu_{rl})\alpha_{rl} + F_{zrr}K_y(\mu_{rr})\alpha_{rr}\right)$$
$$+ l_f F_{zfl}K_y(\mu_{fl})\operatorname{atan}\left(\frac{V_y + rl_f}{V_x - rl_s}\right)$$
$$+ l_f F_{zfr}K_y(\mu_{fr})\operatorname{atan}\left(\frac{V_y + rl_f}{V_x + rl_s}\right) + \Delta M$$
$$- l_f \left[F_{zfl}K_y(\mu_{fl}) + F_{zfr}K_y(\mu_{fr})\right]\delta_{sw}$$
$$= g(\cdot) - \frac{l_f}{R_s}\left[F_{zfl}K_y(\mu_{fl}) + F_{zfr}K_y(\mu_{fr})\right]\delta_s$$

$$(19)$$

where R_s is the steering mechanism gear ratio. Knowing that there are some parametric uncertainties (such as payload and road condition variations) and un-modeled dynamics (such as roll and pitch motions), sliding mode control (SMC) was selected for the yaw rate tracking to enhance system robustness and address the system nonlinearities [15]. Define the sliding surface for the yaw rate tracking control as

$$S_r = r - r_r + \lambda_r\left(\psi - \psi_{ri}\right). \tag{20}$$

The time derivative of the surface is,

$$
\begin{aligned}
\dot{S}_r &= \dot{r} - \dot{r}_r + \lambda_r\dot{\psi} - \lambda_r\dot{\psi}_{ri} \\
&= \frac{1}{I_z}M_z - \dot{r}_r + \lambda_r r - \lambda_r r_r
\end{aligned} \tag{21}
$$

Consider the Lyapunov function candidate

$$V_r = \frac{1}{2}S_r^2 \geq 0. \tag{22}$$

Its derivative is given by

$$\dot{V}_r = S_r\dot{S}_r. \tag{23}$$

In order to ensure the attractiveness of the sliding surface, we need to make $\dot{V}_r \leq -\eta_r|S_r|$. It is easy to verify that the following control law can meet this requirement

$$\delta_s = \frac{I_z\left[\overline{g}(\cdot)/I_z - \dot{r}_r + \lambda_r r - \lambda_r r_r + \eta_r \, \mathrm{sgn}(S_r)\right]}{\frac{l_f}{R_s}\left[\overline{F}_{zfl}K_y\left(\mu_{fl}\right) + \overline{F}_{zfr}K_y\left(\mu_{fr}\right)\right]}, \tag{24}$$

where $\overline{g}$ and $\overline{F}_{z*}$ are the nominal values of g and F_{z*}, respectively, and calculated from (15) and (16) based on GPS/IMU measurement. Thus S_r is asymptotically stable. In other words, $S_r = r - r_r + \lambda_r\left(\psi - \psi_{ri}\right) \to 0$ as $t \to \infty$. From the Final-Value Theorem, we can have $(r - r_r) \to 0$ and $(\psi - \psi_{ri}) \to 0$ as $t \to \infty$. Subsequently, the tracking objectives are fulfilled. In practice, to avoid chattering effect caused by the sign function in the control law, the following saturation function is used to replace the *sgn* function

$$sat\left(\frac{S_r}{\phi_r}\right) = \begin{cases} S_r/\phi_r & \text{if } |S_r| < \phi_r \\ \mathrm{sgn}(S_r/\phi_r) & \text{if } |S_r| \geq \phi_r \end{cases}. \tag{25}$$

IV. SIMULATION STUDIES

The trajectory tracking control system is implemented in Simulink™ with the validated AGV full-vehicle model constructed in CarSim®.

A. Autonomous Operation on a Race Track

The developed AGV control system is evaluated to follow the trajectory of a race track. The target AGV speed is set constant as 50 km/h. A proportional-integral (PI) controller is used to track the desired vehicle speed. For comparison purpose, another AGV system where steering command is connected with vehicle localized lateral position error by a PI controller is also evaluated using the identical vehicle model.
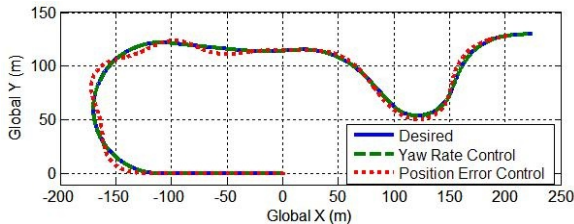

Fig. 7. Comparison of global trajectories for different AGV control approaches.

Fig. 7 shows the vehicle global trajectories, as can be seen, the AGV using yaw rate control can almost perfectly track the desired trajectory even with sharp turns at 50 km/h while the position error based control exhibits some unstable oscillations during turnings. Vehicle planar motions and roll rate are also shown in Fig. 8 for these two different AGV control systems. The AGV with yaw rate control well outperforms the position error based control in terms of maintaining stable yaw and roll motions. Notice that the vehicle lateral speed is ignorable compared with V_x.
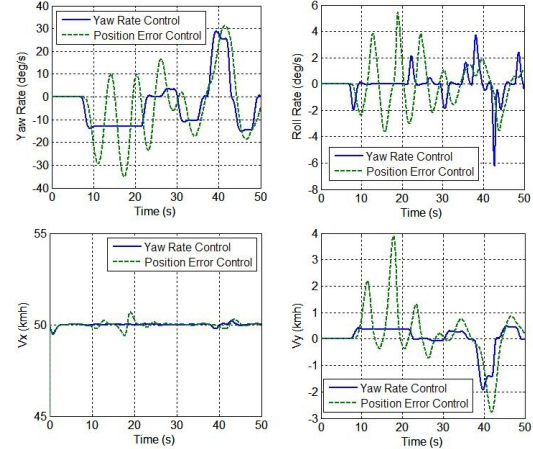

Fig. 8. Comparison of vehicle planar motions and roll rate.

The commanded vehicle steering hand-wheel signals for these two different controllers are plotted together in Fig.9.
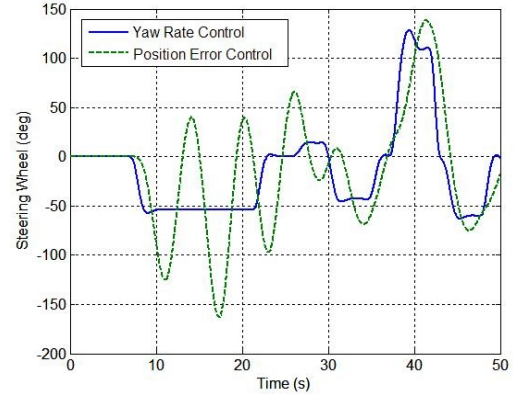

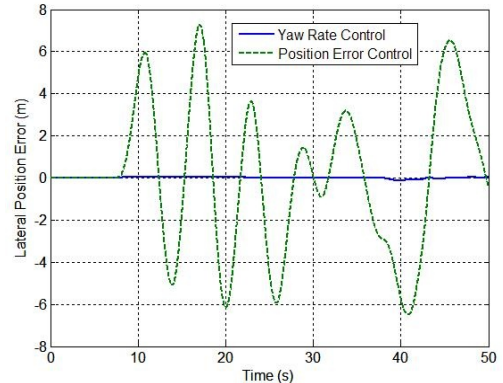Fig. 9. Commanded steering wheel positions of the two AGV controllers.

Fig. 10. Comparison of the body-fixed lateral tracking positions.

The difference of the localized lateral tracking errors

for the two AGV controllers is significant (Fig. 10). The peak error for the AGV with yaw rate control is 0.06 m but 7.27 m for the position error based AGV control during the sharp turns at 50 km/h.

AGV behaviors during a sharp turn are captured from the simulation as shown in Fig. 11, in which the dash central line is the desired trajectory. Blue SUV is the AGV with yaw rate control and the red SUV is the AGV using position error based control. As we can see, the yaw rate control can maintain the vehicle stability well.
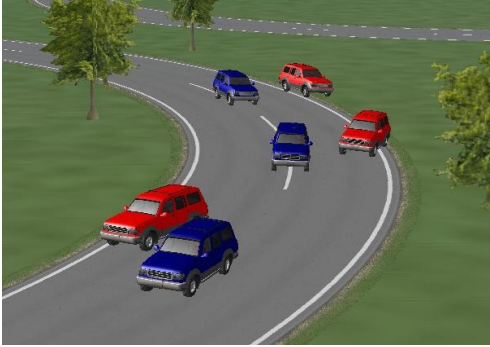

Fig. 11. Comparison of the AGV behaviors at a sharp turn.

B. Trajectory Tracking with an Initial Offset

To further exhibit the performance of the proposed AGV control system, another scenario where the starting point was intentionally offset by 1 m was conducted. The results are shown in Fig. 12. One can find that the AGV with yaw rate controller can quickly converge to the desired trajectory while the position error controller cannot.
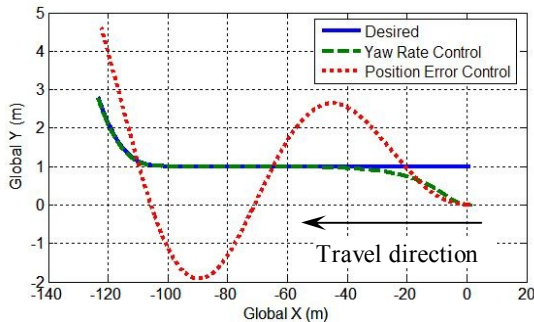

Fig. 12. Comparison of the global trajectories of the two AGV control systems during trajectory tracking with an initial position offset.

It is worthy to reiterate that the control architecture proposed in this paper breaks the direct connection between trajectory tracking and steering that is usually adopted for AGV systems. Therefore, not only steering control but also other advanced vehicle dynamics (planar motion/yaw rate) control approaches such as differential braking and torque-vectoring can be seamlessly incorporated into the AGV control to expand the AGV operational envelope to high-speed and safe operation.

V. FUTURE WORK AND CONCLUSIONS

In this paper, an AGV trajectory tracking control system is proposed. The control law employs the measurement from readily available GPS/IMU to control vehicle yaw rate to track the desired trajectory. The

separation between vehicle position tracking error and steering command makes it easy to incorporate vehicle dynamics control to expand the operational envelope. Simulation results based on a high-fidelity full-vehicle model show the benefits of the control system in terms of perfect tracking and vehicle stability during severe maneuvers.

We are in the process of implementing the control law on the SSTI AGV platform for experimental evaluations. Other yaw rate control systems utilizing advanced sensing and actuation systems such as vision, lidar, GPS/IMU, differential braking will be investigated as well.

REFERENCES

[1] P. Falcone, F. Borrelli, J. Asgari, H. Tseng, and D. Hrovat, "Predictive Active Steering Control For Autonomous Vehicle Systems," *IEEE Transactions on Control Systems Technology*, Vol. 15, No. 3, pp. 566 – 579, 2007.

[2] S. L. Tan and J. Gu, "Investigation of Trajectory Tracking Control Algorithms for Autonomous Mobile Platforms: Theory and Simulation," *Proceedings of the IEEE International Conference on Mechatronics & Automation*, pp. 934 – 939, 2005.

[3] G. Hoffmann, C. Tomlin, M. Montemerlo, and S. Thrun, "Autonomous Automobile Trajectory Tracking for Off-Road Driving: Controller Design, Experimental Validation and Racing," *Proceedings of the 2007 American Control Conference*, pp. 2296 – 2301, 2007.

[4] R. Rajamani, C. Zhu, and L. Alexander, "Lateral Control of a Backward Driven Front-Steering Vehicle," *Control Engineering Practice*, Vol. 11, pp. 531 – 540, 2003.

[5] R. Solea and U. Nunes, "Trajectory Planning with Velocity Planner for Fully-Automated Passenger Vehicles," *Proceedings of the 2006 IEEE Intelligent Transportation Systems Conference*, pp. 474 – 480, 2006.

[6] R. Rajamani, H.S. Tan, B. K. Law, and W. B. Zhang, "Demonstration of Integrated Longitudinal and Lateral Control for the Operation of Automated Vehicles in Platoons," *IEEE Transactions on Control Systems Technology*, Vol. 8, No. 4, pp. 695 – 708, 2000.

[7] P. Heinzl, P. Lugner, and M. Plochl, "Stability Control of a Passenger Car by Combined Additional Steering and Unilateral Braking," Vehicle System Dynamics Supplement, Vol. 37, pp. 221 – 233, 2002.

[8] J. Fredriksson, J. Andreasson, and L. Laine, "Wheel Force Distribution for Improved Handling of a Hybrid Electric Vehicle Using Nonlinear Control," *Proceedings of 43rd IEEE Conference on Decision and Control*, pp. 4081 – 4086, 2004.

[9] J. Wang and R. G. Longoria, "Coordinated Vehicle Dynamics Control with Control Distribution," *Proceedings of the 2006 American Control Conference*, pp. 5348 – 5353, 2006.

[10] J. Wang and R. G. Longoria, "Combined Tire Slip and Slip Angle Tracking Control for Advanced Vehicle Dynamics Control Systems," *Proceedings of the 45th IEEE Conference on Decision and Control*, pp. 1733 – 1738, 2006.

[11] J. Wang, J. M. Solis, and R. G. Longoria, "On the Control Allocation for Coordinated Ground Vehicle Dynamics Control Systems," *Proceedings of the 2007 American Control Conference*, pp. 5724 – 5729, 2007.

[12] Y.J. Kanayama, Y. Kimura, F. Miyazaki, and T. Noguchi, "A Stable Tracking Control Method for an Autonomous Mobile Robot," *Proceedings of the IEEE International Conference on Robotics and Automation*, pp. 384 – 389, 1990.

[13] J. Wang, L. Alexander, and R. Rajamani, "Friction Estimation on Highway Vehicles Using Longitudinal Measurements," *Journal of Dynamic Systems, Measurement, and Control*, Vol. 126, Issue 2, pp. 265 – 275, 2004.

[14] D., Bevly, J. Gerdes, C. Wilson, and G. Zhang, "The Use of GPS Based Velocity Measurements for Improved Vehicle State Estimation," *Proceedings of 2000 the American Control Conference*, pp. 2538 – 2542, 2000.

[15] V. I. Utkin, J. Gulder, and S. Ma, *Sliding Mode Control in Electromechanical Systems*, Taylor & Francis Inc., PA, 1999.